Separation Science and Technology
Publication details, including instructions for authors and subscription information:
http://www.informaworld.com/smpp/title~content=t713708471

PERFORMANCE CHARACTERISTICS OF NOVEL OPEN PARALLEL PLATE SEPARATOR

Blanca H. Lapizco-Encinas[a]; Neville G. Pinto[a]
[a] Department of Chemical Engineering, University of Cincinnati, Cincinnati, OH, U.S.A.

Online publication date: 08 May 2002

To cite this Article Lapizco-Encinas, Blanca H. and Pinto, Neville G.(2002) 'PERFORMANCE CHARACTERISTICS OF NOVEL OPEN PARALLEL PLATE SEPARATOR', Separation Science and Technology, 37: 12, 2745 — 2762
To link to this Article: DOI: 10.1081/SS-120005464
URL: http://dx.doi.org/10.1081/SS-120005464

SEPARATION SCIENCE AND TECHNOLOGY, 37(12), 2745–2762 (2002)

PERFORMANCE CHARACTERISTICS OF NOVEL OPEN PARALLEL PLATE SEPARATOR

Blanca H. Lapizco-Encinas and Neville G. Pinto*

Department of Chemical Engineering, University of Cincinnati, 696 Rhodes Hall, P.O. Box 210171, Cincinnati, OH 45221-0171

ABSTRACT

A numerical model has been developed to describe the characteristics of the recently developed micro open parallel plate separator (μOPPS). This model solves the mass-balance equation for a single solute within a microchannel with a rectangular flow cross-section, and accounts for the velocity profile in the channel. It is shown that the separation characteristics are sensitive to the concentration and velocity gradients along the depth—a factor that has been neglected in the past. An empirical expression has been developed for the reduced plate height of the μOPPS. It has been shown that estimation of performance parameters using an equivalent radius in equations developed for a circular cross-section gives erroneous predictions.

Key Words: Adsorption; Modeling; Ion-exchange; Micro-separator; Microchannel

*Corresponding author. Fax: (513) 556-3473; E-mail: neville.pinto@uc.edu

INTRODUCTION

Modern micromechanical fabrication techniques offer new opportunities for chemical separations. The separation of a sample into its components is often an essential step in chemical analysis,[1] and miniaturization offers significant potential advantages including decreased analysis time, sample consumption, and waste solvent production, lower cost due to reduction of sample and reagents, reduced weight and volume, the opportunity for multiple, parallel separations, and reduced band broadening due to smaller dimensions.[2–4]

Miniaturization of analytical instruments through micro-electro-mechanical-systems (MEMS) technology was first implemented 20 years ago.[5] In recent years, there has been a spurt of activity in the development of "laboratories-on-a-chip." Much of this work has focused on capillary electrophoresis[6–9] and electrokinetic capillary chromatography.[10–13]

The best analytical columns for liquid chromatography (LC) are open tubular columns (OTC), which are the true analogues of capillary gas chromatographic columns. The main advantage of OTC over packed capillary columns is its larger permeability.[14] For good mass-transfer efficiency, an OTC must have an extremely small diameter (less than 5 μm), yet the diameter should be large enough to avoid overloading.[15] The open parallel plate separator (OPPS) geometry, which is based on a rectangular flow cross-section area, has been suggested as an alternative. The narrow width dimension preserves the favorable mass-transfer characteristic, while the long depth dimension allows an increase in the column volume to avoid overloading. In addition, the larger flow cross-section area enables separations with high flow rate at a lower pressure drop.

Using MEMS it is possible to fabricate an OPPS on a silicon wafer. We have recently reported the fabrication of an integrated ion-exchange separator and detector (μOPPS).[16,17] It has been demonstrated with this prototype that small ions can be effectively separated and detected by the device.

To guide the developments of future versions of the μOPPS, and to identify advantages and disadvantages in comparison to a separator with a circular cross-section area, i.e., a micro open tubular separator (μOTS), it is useful to develop a model for the μOPPS. While columns having a circular or trapezoidal flow cross-section have been studied extensively,[8,10,14,18–22] there is limited modeling work on OPPS. Golay[18] proposed a model for circular and square cross-section columns, but he focused on gas chromatography (GC). Giddings et al.[15] have developed equations that describe the performance of OPPS in comparison to the OTS in LC. A set of experimental data were presented for OPPS, and compared to model predictions. Discrepancies in plate height (H) as high as a factor of 40 was observed. Vahey et al.[23] have applied Giddings model to a chromatographic analyzer with a rectangular cross-section flow area. They reported good agreement between the theory and the experimental data, though the linear

velocities used were low (0.009–0.018 cm/sec), compared to those used by Giddings (0.1–1.0 cm/sec).[15] Zhang and Regnier[24] have also studied the effects of column geometry. A three-dimensional random walk model for a micro-chromatographic system with electroosmotic flow was developed assuming a flat velocity profile.

In this paper, we present a detailed model for OPPS in LC. It has been shown through numerical simulations that nonsymmetry in the flow cross-section, and the velocity and concentration gradients along the channel depth influence the chromatographic response.

THEORY

Model for Open Parallel Plate Separator

A schematic representation of the OPPS is shown in Fig. 1. It is assumed that the flow regime in this channel is laminar and fully developed with negligible end effects. For this case Spangler[25] has shown that the velocity profile is given by:

$$v_y = -3v_{\text{avg}}\left(\frac{b^2+d^2}{b^2d^2}\right)\left(\frac{(x^2-b^2)(z^2-d^2)}{(x^2-b^2)+(z^2-d^2)}\right) \tag{1}$$

where v_y is the linear velocity in the fluid flow (length) direction, v_{avg} the average linear velocity, b the microchannel half width, d the microchannel half depth, x and z are the positions along the microchannel width and depth, respectively.

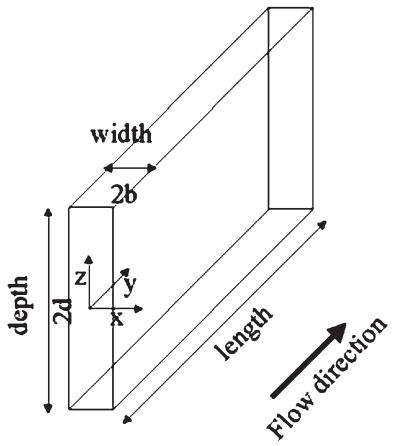

Figure 1. Schematic representation of an OPPS.

Adsorption of the solute is assumed to take place on the surfaces defined by the depth and length dimensions (side surfaces) of the channel, while the surfaces defined by the width and the length (top and bottom surfaces) are assumed to be inactive. This choice is based on the experimental μOPPS developed earlier.[16,17] The top/bottom surfaces are inert, while the side surfaces are activated for ion-exchange. It is further assumed that the adsorption (or ion-exchange) step is instantaneous, relative to the mass-transfer rate. The predominant mass-transfer resistance is in the liquid phase, since the surface is assumed to be nonporous and ideally two-dimensional. Upon injection, the sample is assumed to be evenly distributed along the channel cross-section, and the fluid density is assumed constant. Since the amount of solute injected is small (nL), adsorption equilibrium is described by the linear equation:

$$q^* = aC \tag{2}$$

where q^* is the equilibrium concentration of solute in the stationary phase, a is the linear isotherm coefficient, and C is the solute concentration in the mobile phase.

With these assumptions it can be shown that a mass balance for a solute in the channel is:

$$\frac{\partial C}{\partial t} - 3\frac{\partial C}{\partial y} v_{\text{avg}} \left(\frac{b^2 + d^2}{b^2 d^2}\right) \left(\frac{(x^2 - b^2)(z^2 - d^2)}{(x^2 - b^2) + (z^2 - d^2)}\right) = D\left(\frac{\partial^2 C}{\partial x^2} + \frac{\partial^2 C}{\partial y^2} + \frac{\partial^2 C}{\partial z^2}\right) \tag{3}$$

where D is the solute's diffusion coefficient in the fluid.

For convenience the following dimensionless variables are defined:

$$\text{Dimensionless time}: \quad \tau = \frac{v_{\text{avg}} t}{L} \quad \theta_X = \frac{v_{\text{avg}} b^2}{DL} \quad \theta_Z = \frac{v_{\text{avg}} d^2}{DL} \tag{4}$$

$$\text{Dimensionless spatial position}: \quad X = \frac{x}{b} \quad Y = \frac{y}{L} \quad Z = \frac{z}{d} \tag{5}$$

$$\text{Peclet number}: \quad Pe = \frac{v_{\text{avg}} L}{D} \tag{6}$$

where L is the length of the microchannel.

Re-writing Eq. (3) in terms of these parameters:

$$\frac{\partial C}{\partial \tau} - 3\frac{\partial C}{\partial Y} \left(\frac{b^2 + d^2}{d^2}\right) \left(\frac{(X^2 - 1)(Z^2 - 1)}{\frac{b^2}{d^2}(X^2 - 1) + (Z^2 - 1)}\right) = \frac{1}{\theta_X}\frac{\partial^2 C}{\partial X^2} + \frac{1}{Pe}\frac{\partial^2 C}{\partial Y^2} + \frac{1}{\theta_Z}\frac{\partial^2 C}{\partial Z^2} \tag{7}$$

For isocratic elution chromatography, with no solute present in the channel at the start of the separation, the following initial and boundary conditions apply:

$$\text{Initial condition}: \quad \text{At} \quad \tau = 0 \quad C(X, Y, Z) = 0$$
$$0 \le X \le 1, 0 \le Y \le 1, 0 \le Z \le 1 \tag{8}$$

Boundary conditions:

At the channel wall (side surfaces) the solute diffusion flux in the liquid is equal to accumulation at the surface due to adsorption:

$$\text{at} \quad X = 1 \quad -D\frac{\partial C}{\partial x}\bigg|_{x=b} = \frac{\partial q^*}{\partial t} \tag{9}$$

After substitution of the equilibrium condition [Eq. (2)], [Eq. (9)] becomes

$$\frac{\partial C}{\partial X}\bigg|_{X=1} = -\frac{a}{b\theta_X}\frac{\partial C}{\partial \tau}\bigg|_{X=1} \tag{10}$$

It is usual to assume that there is no concentration gradient at the channel exit. Thus,

$$\text{at} \quad Y = 1 \quad \frac{\partial C}{\partial Y}\bigg|_{Y=1} = 0 \tag{11}$$

Since the top and bottom cover plates of the OPPS are assumed inert, there is no flux at these plates. Thus,

$$\text{at} \quad Z = 1 \quad -D\frac{\partial C}{\partial Z}\bigg|_{Z=1} = 0 \tag{12}$$

From symmetry,

$$\text{at} \quad X = 0, \quad \frac{\partial C}{\partial X}\bigg|_{X=0} = 0 \tag{13}$$

and

$$\text{at} \quad Z = 0, \quad \frac{\partial C}{\partial Z}\bigg|_{Z=0} = 0 \tag{14}$$

Finally, for an isocratic elution experiment,

$$\text{at} \quad Y = 0, \quad C(X, 0, Z) = C_{\text{feed}}, \quad 0 < \tau \le \tau_{\text{feed}} \tag{15}$$

$$C(X, 0, Z) = 0, \quad \tau > \tau_{\text{feed}} \tag{16}$$

where τ_{feed} is the dimensionless feed time and C_{feed} is the feed solute concentration.

In order to solve Eq. (7), the numerical method of finite differences was applied. Forward difference was used for the first-order temporal derivative and central difference for all the spatial derivatives. In order to obtain a stable solution, the alternating direction implicit scheme was employed. This scheme divides each time interval between the number of spatial directions (in this case three directions): channel width, depth, and length. Each spatial direction is represented by a tridiagonal matrix of equations, which is solved using the LU-decomposition method (tridiagonal matrix method).

The particular scheme used is the Peaceman–Rachford algorithm that is described in detail elsewhere.[26] The numerical method uses four indices: n for time, j, k, and m for width, length, and depth, respectively. For convenience, the following finite difference terms are defined:

$$R_x = \frac{\Delta\tau}{\theta_X \Delta X^2} \quad R_y = \frac{\Delta\tau}{Pe\Delta Y^2} \quad R_z = \frac{\Delta\tau}{\theta_Z \Delta Z^2} \quad S_y = -\frac{3\Delta\tau}{2\Delta Y}\left(\frac{b^2}{d^2}+1\right)$$

$$\delta_x^2 C_{j,k,m}^n = C_{j-1,k,m}^n - 2C_{j,k,m}^n + C_{j+1,k,m}^n$$

$$\delta_y^2 C_{j,k,m}^n = C_{j,k-1,m}^n - 2C_{j,k,m}^n + C_{j,k+1,m}^n$$

$$\delta_z^2 C_{j,k,m}^n = C_{j,k,m-1}^n - 2C_{j,k,m}^n + C_{j,k,m+1}^n$$

$$\delta_{y0} C_{j,k,m}^n = C_{j,k-1,m}^n - C_{j,k+1,m}^n$$

Substituting in Eq. (7):

$$C_{j,k,m}^{n+1} - C_{j,k,m}^n + \delta_{y0} C_{j,k,m}^n S_y \left(\frac{(X_j^2-1)(Z_m^2-1)}{\frac{b^2}{d^2}(X_j^2-1)+(Z_m^2-1)}\right) = R_x\delta_x^2 C_{j,k,m}^n + R_y\delta_y^2 C_{j,k,m}^n + R_z\delta_z^2 C_{j,k,m}^n \tag{17}$$

The Peaceman–Rachford algorithm breaks Eq. (17) into three parts:

$$\left(1-\frac{R_x}{3}\delta_x^2\right)C_{j,k,m}^{n+1/3} = \left(1+\frac{R_y}{3}\delta_y^2+\frac{R_z}{3}\delta_z^2\right)C_{j,k,m}^n - \delta_{y0} C_{j,k,m}^n \frac{S_y}{3}\left(\frac{(X_j^2-1)(Z_m^2-1)}{\frac{b^2}{d^2}(X_j^2-1)+(Z_m^2-1)}\right) \tag{18}$$

$$\left(1-\frac{R_y}{3}\delta_y^2\right)C_{j,k,m}^{n+2/3}=\left(1+\frac{R_x}{3}\delta_x^2+\frac{R_z}{3}\delta_z^2\right)C_{j,k,m}^{n+1/3}-\delta_{y0}C_{j,k,m}^{n+1/3}\frac{S_y}{3}\left(\frac{(X_j^2-1)(Z_m^2-1)}{\frac{b^2}{d^2}(X_j^2-1)+(Z_m^2-1)}\right) \tag{19}$$

$$\left(1-\frac{R_z}{3}\delta_z^2\right)C_{j,k,m}^{n+1}=\left(1+\frac{R_x}{3}\delta_x^2+\frac{R_y}{3}\delta_y^2\right)C_{j,k,m}^{n+2/3}-\delta_{y0}C_{j,k,m}^{n+2/3}\frac{S_y}{3}\left(\frac{(X_j^2-1)(Z_m^2-1)}{\frac{b^2}{d^2}(X_j^2-1)+(Z_m^2-1)}\right) \tag{20}$$

Each of these equations was solved in a separate numerical subroutine.

Model for Open Tubular Separator

A numerical simulator was built to predict the performance for the OTS, using the same mathematical scheme used for the OPPS model. The OTS model is based on the same assumptions as the OPPS model, except that there is no inert surface. The mass-balance equation for a single component in the OTS gives:

$$\frac{\partial C}{\partial \tau}+2(1-r^2)\frac{\partial C}{\partial Y}=\frac{1}{Pe}\frac{\partial^2 C}{\partial Y^2}+\frac{1}{\theta_r}\frac{1}{r}\frac{\partial C}{\partial r}+\frac{1}{\theta_r}\frac{\partial^2 C}{\partial r^2} \tag{21}$$

where r is the dimensionless position in the radial direction.

RESULTS AND DISCUSSION

Simulations were performed using the parameters listed in Table 1, unless otherwise stated. The channel length corresponds to the length of the prototype μOPPS developed earlier.[16,17] The solute is assumed to be KBr, exchanging on a polyethyleneimine (PEI)-activated surface. The diffusion coefficient was obtained from Ref.[27] and the linear adsorption isotherm coefficient was calculated by Kang.[28] Based on this selection, the sample volume was fixed at 4% of the channel volume in all cases.

Table 1. Simulation Parameters Used for Both Open Parallel Plate Separator and Open Tubular Separator

Micro-channel Length (L)	3 (cm)
Linear velocity (v_{avg})	0.2 (cm/sec)
Diffusion coefficient (D)	2×10^{-5} (cm^2/sec)
Adsorption isotherm coefficient (a)	0.00792 (cm)
Sample concentration (C_{feed})	1000 (μmol/cm^3)
Sample volume (VF)	4 (% of channel volume)

The following parameters are important to quantify the separation characteristics: the reduced plate height [Eq. (22)] and the separation impedance [Eq. (23)].[29]

$$h = \frac{H}{d_{eq}} \tag{22}$$

$$E = \frac{T_R \Delta P}{N^2 \mu (1 + k')} \tag{23}$$

In these equations, the equivalent diameter for the OPPS, number of plates and the pressure drop are calculated as follows:

$$d_{eq} = \frac{4bd}{b + d} \tag{24}$$

$$N = 5.54 \left(\frac{T_R}{w_h} \right)^2 \tag{25}$$

$$\Delta P = \frac{3 \mu L v_{avg}}{b^2} \tag{26}$$

where T_R is the retention time, w_h the peak width at half of the height of the peak, μ the mobile phase viscosity, and k' the column capacity factor.

One of the purposes for the OTS simulations was to compare the results with predictions of the OTS equation of Giddings et al.:[15]

$$h_{OTS} = (6R^2 - 16R + 11) \frac{r_C}{D} \frac{v_{avg}}{48} \tag{27}$$

where, h_{OTS} is the reduced plate height for the OTS, R is the retention ratio, D is the diffusion coefficient, and v_{avg} is the average linear velocity in the OTS. The validity of this equation is well established, and, good correspondence with numerical results will validate the numerical procedure selected. Figure 2 shows

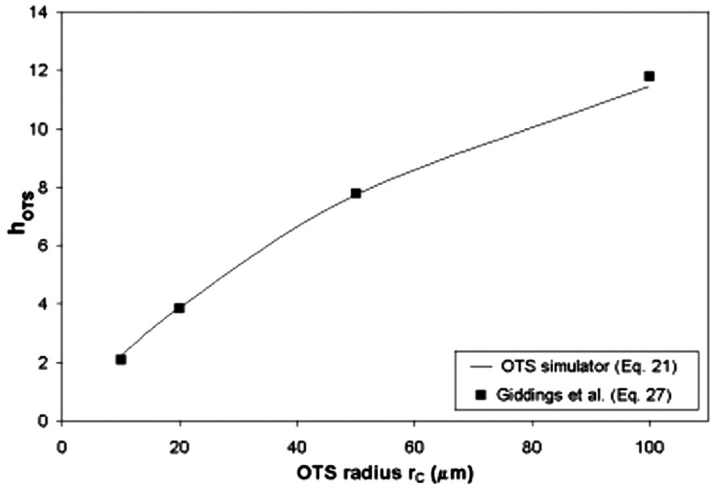

Figure 2. Comparison of reduced plate height predictions in OTS from the simulations and Giddings equation.[15]

a comparison of the predictions from this equation with those obtained from Eq. (21). As can be seen, there is very good agreement between the two predictions.

A similar comparison was performed for the OPPS. Results from numerical solutions of Eq. (7) were compared to predictions from the plate-height equation for OPPS given by Giddings et al.:[15]

$$h_{\mathrm{OPPS}} = \frac{2(35R^2 - 84R + 51)}{d_{\mathrm{eq}}} \frac{b^2}{D} \frac{v_{\mathrm{avg}}}{105} \tag{28}$$

It is important to note that Eq. (28) was derived by analogy with Eq. (27). That is, the depth-to-width ratio was not accounted for. Since the OPPS has a flow cross-section closest to the OTS when the depth-to-width ratio is equal to one, it is expected that Eq. (28) is best applicable when the flow cross-section is square.

Figure 3 shows a comparison of the results obtained from Eqs. (7) and (28) for a square flow cross-section. It is clear that the reduced plate-height values predicted by the two equations do not match, in strong contrast to the excellent correspondence in Fig. 2. Equation (28) is predicting much lower h_{OPPS} values. It is significant that in comparing the predictions of Eq. (28) to experimental data, a similar over-prediction of performance was reported.[15] This and the results of Fig. 3 suggest that even with the restriction of a square cross-section, Eq. (28) is not valid.

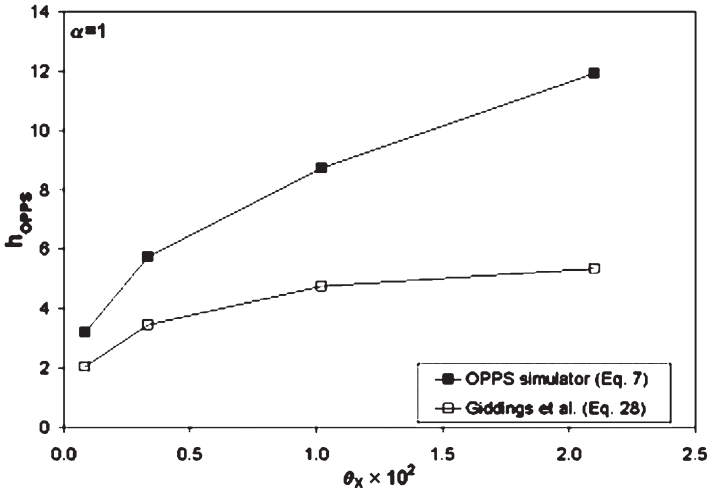

Figure 3. Comparison of reduced plate height predictions in OPPS with square flow cross-section from simulations and Giddings equation.[15]

As was mentioned earlier, a limitation of Eq. (28) is that it does not specifically account for the influence of the depth-to-width ratio (rectangular cross-sections). This ratio can be most generally defined in terms of the dimensionless times θ_Z and θ_X as:

$$\frac{\theta_Z}{\theta_X} = \left(\frac{d}{b}\right)^2 = \alpha \tag{29}$$

Shown in Fig. 4 is the effect of α on the reduced plate height, as predicted by Eq. (7). The range selected (1–400) corresponds to values that can easily be achieved in open parallel-plate systems.[15,16] It is seen that α has a strong influence on performance. Generally, narrower channels are less strongly influenced by this ratio. Also, at high values of α the performance is only weakly influenced by changes in this parameter. However, there is clearly a region where performance is a strong function of α, indicating that a suitable equation for the plate height must in general account for the influence of this parameter.

The separation impedance, E [Eq. (23)] is a useful parameter to characterize performance for the selection of the optimal geometry since it incorporates the number of plates with the cost (in terms of ΔP) for achieving a separation. Shown in Fig. 5 is the dependence of the separation impedance on the OPPS geometry. Two factors are significant. First it is apparent that identical values of E can be obtained with different geometric ratios. Secondly, it is predicted that with the

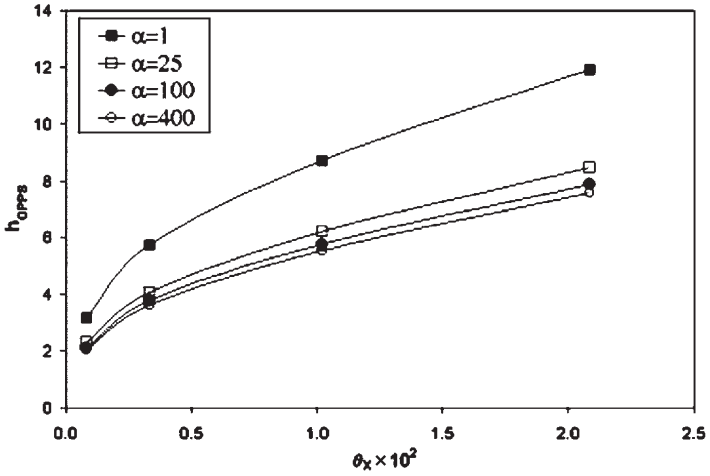

Figure 4. Effect of depth-to-width ratio on h_{OPPS}.

proper selection of device dimensions and fluid flow velocity, excellent separation impedances in the range of 100–200 are achievable with the OPPS.

The dependence of the performance of the OPPS on both θ_X and θ_Z points to the problem in the derivation of Eq. (28). This equation was derived, by analogy with the OTS plate equation [Eq. (27)]. It was concluded[15] that

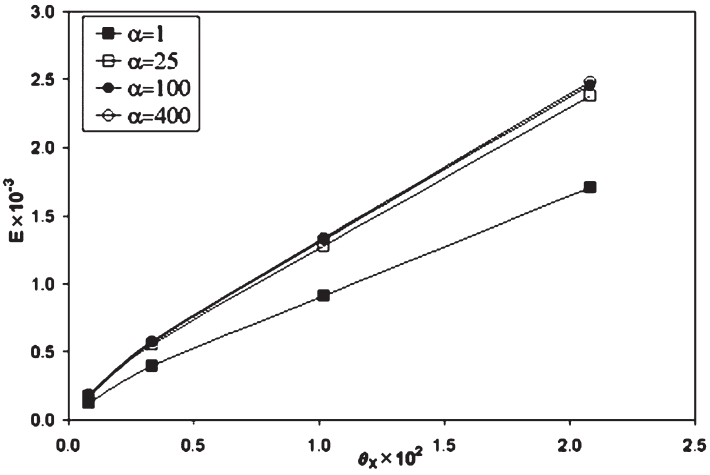

Figure 5. Effect of depth-to-width ratio on E.

equivalent performance can be expected from the OTS and OPPS if the width of the OPPS is comparable to the radius of the OTS ($b = 0.7\, r_C$). It was rationalized that the slightly smaller critical dimension for OPPS is required to compensate for better mass-transfer accessibility in OTS. Besides neglecting the influence of α, as was discussed earlier, one other assumption is implicitly made. The OTS equation is based on the assumption that the concentration gradient within the flow cross-section can be neglected. This assumption is valid for the OTS because of the symmetry of the circular cross-section, which in effect allows the substitution of the radial profile with an effective concentration at that cross-section. The situation is different in an OPPS, since the cross-section is not symmetric about the central point.

Figures 6 and 7 show typical concentration profiles predicted for the flow cross-section in the OPPS. In each figure, the concentration profiles are shown at two locations: one-tenth the channel length (A), and at the end of the channel (B). Figure 6 is the concentration profile for a θ_X value of 0.00083, corresponding to a narrow channel (10 μm width), and Fig. 7 is for a θ_X value of 0.021, a relatively wider channel (50 μm). It can be seen that for the narrower channel at the upstream end (Fig. 6A), while the concentration does change across a cross-section, the percentage change is small. Furthermore, at the channel outlet (Fig. 6B) the small variation is eliminated. Also, the influence of α is seen to be weak. Thus, the concentration profile has little influence, and the use of an average concentration is justified.

For wider channels the story is different, as shown in Fig. 7. The concentration changes significantly along the width at every length location, and

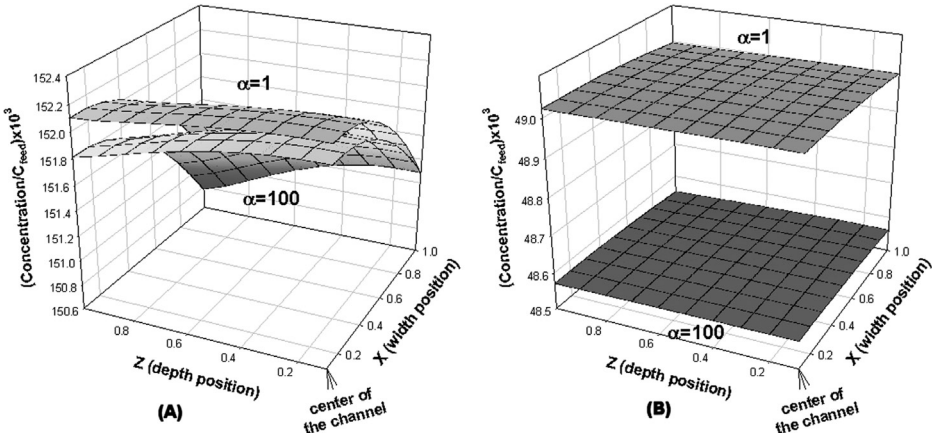

Figure 6. Concentration profile at a cross-section for a 10 μm width channel (shown for half of the channel cross-section) at: (A) 10% of channel length, and (B) 100% channel length.

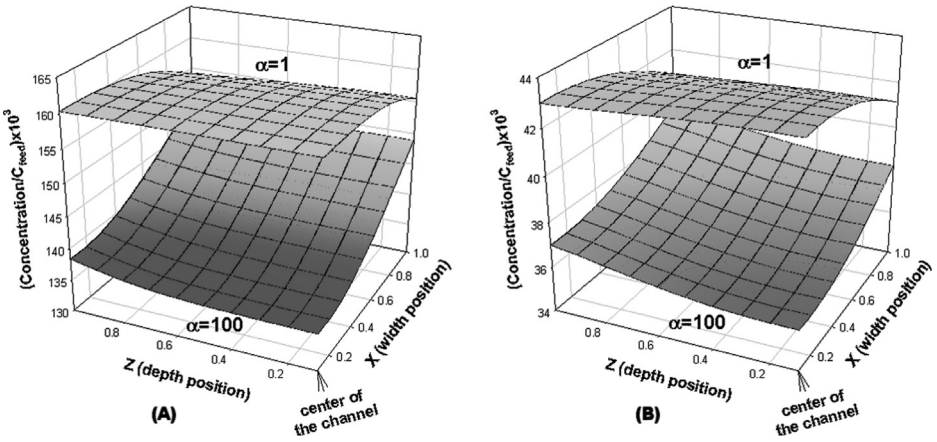

Figure 7. Concentration profile at a cross-section for a 50 μm width channel (shown for half of the channel cross-section) at: (A) 10% of channel length, and (B) 100% channel length.

the profile is strongly asymmetric. For example, for the case considered, the concentration within a cross-section varies a minimum of 10% at every cross-section. Furthermore, the shape of the profile is a strong function of α. For $\alpha = 1$ the profile is concave upward, while for $\alpha = 100$ it is convex upward. The asymmetry in the profile and significant variation in concentration implies that for wider channels the use of an average concentration is not justified. Furthermore, since the shape of the profile, and, therefore, the driving force for mass transfer, depends on α this term must be factored into the equation for plate height.

It is useful to develop an equation for the plate height that will incorporate the influence of channel shape. Since an analytical solution cannot be obtained for Eq. (7), it is not possible to derive such an expression.

Using Eq. (7), isocratic elutions were simulated for a wide range of conditions. From these results and a dimensional analysis, an empirical expression for reduced plate height was developed:

$$h_{\mathrm{OPPS}} = \left(\frac{4.81Pe^{0.27}}{\alpha} + 3.37Pe^{0.35}\right)\theta_X^{0.92}\beta \tag{30}$$

where

$$\beta = \frac{a}{b} \tag{31}$$

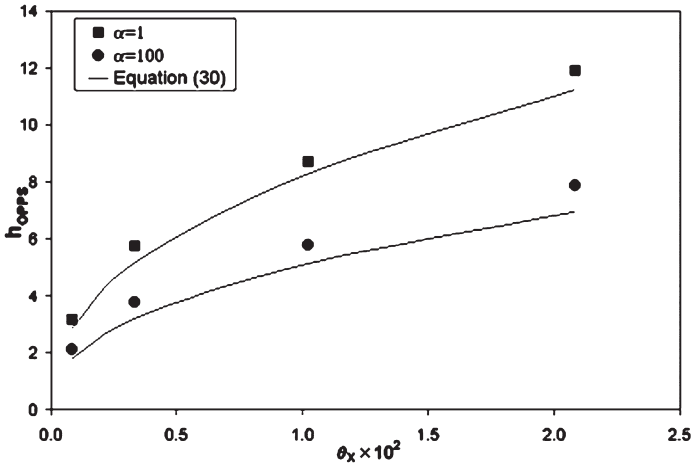

Figure 8. Characterization of OPPS efficiency with empirical reduced plate height [Eq. (30)].

A typical comparison of the values predicted by Eq. (30) and simulations is shown in Fig. 8. The ranges of conditions used for developing Eq. (30) are: $6.24 \times 10^{-4} < \theta_X < 0.042$; $1 < \alpha < 1 \times 10^6$; $1.944 < \beta < 9.72$; and $2.25 \times 10^4 < Pe < 6 \times 10^4$. Over 160 simulations were performed within this range of conditions and the average absolute error was found to be 11%, with a standard deviation of 10%.

CONCLUDING REMARKS

A mathematical model has been developed to describe the elution of a single solute in an OPPS under linear equilibrium conditions. It has been shown that the velocity and concentration gradients along the depth influence the chromatographic characteristics. In general, channels that are most symmetric (α closer to 1) are slightly less efficient in terms of the reduced plate height, but to some extent, are more efficient in terms of separation impedance. Due to the effects of the velocity and concentration gradients on the performance, methods in the literature based on equating the OPPS-to-OTS with an equivalent radius are not recommended.

By using the predictions of the OPPS simulator an empirical equation has been developed for predicting plate-height in OPPS. It has been found that this equation accurately characterizes the results from the OPPS simulator over a wide range of conditions.

NOMENCLATURE

a	linear isotherm coefficient (cm)
b	microchannel half width (cm)
C	solute concentration in the mobile phase (μmol/cm^3)
C_{feed}	feed solute concentration (μmol/cm^3)
d	microchannel half depth (cm)
D	diffusion coefficient in solution (cm^2/sec)
d_{eq}	microchannel equivalent diameter (cm)
E	separation impedance (dimensionless)
h_{OPPS}	reduced plate height of the OPPS (dimensionless)
h_{OTS}	reduced plate height of the OTS (dimensionless)
H_{OPPS}	plate height of the OPPS (cm)
k'	capacity factor (dimensionless)
L	microchannel length (cm)
N	number of theoretical plates (dimensionless)
Pe	Peclet number (dimensionless)
q^*	equilibrium concentration of solute in the stationary phase (μmol/cm^2)
r	radial position (dimensionless)
R	retention ratio (dimensionless)
r_{C}	microcolumn radius (cm)
t	time (sec)
T_{R}	retention time (sec)
v_y	linear velocity along the length (cm/sec)
v_{avg}	average velocity along the length (cm/sec)
w_{h}	width at half height of the peak (sec)
x	position along the microchannel width (cm)
X	dimensionless position along the microchannel width
y	position along the microchannel length (cm)
Y	dimensionless position along the microchannel length
z	position along the microchannel depth (cm)
Z	dimensionless position along the microchannel depth
Greek symbols	
α	θ_z/θ_X ratio (dimensionless)
β	a/b ratio (dimensionless)
ΔP	pressure drop (psia)
μ	mobile phase viscosity (cp)
θ_X	dimensionless time [Eq. (4)]
θ_z	dimensionless time [Eq. (4)]
τ	dimensionless time [Eq. (4)]
τ_{feed}	dimensionless feed time

ACKNOWLEDGMENT

The authors wish to acknowledge gratefully the financial support provided by CONACYT Mexico in the form of a fellowship to Ms. Blanca H. Lapizco-Encinas. Helpful suggestions from Dr. Dave Robertson of Ohio Supercomputer Center for improving computational efficiency are gratefully acknowledged.

REFERENCES

1. Effenhauser, C.S. Integrated Chip-Based Microcolumn Separation Systems. In *Microsystem Technology in Chemistry and Life Sciences*; Manz, A., Becker, H., Eds.; Springer: New York, 1998; 52–82.
2. He, B.; Regnier, F. Microfabricated Liquid Chromatography Columns Based on Collocated Monolith Support Structures. J. Pharm. Biomed. Anal. **1998**, *17*, 925–932.
3. Fintschenko, Y.; van den Berg, A. Silicon Microtechnology and Microstructures in Separation Science. J. Chromatogr. A **1998**, *819*, 3–12.
4. Jacobson, S.C.; Hergenroder, R.; Koutny, L.B.; Ramsey, J.M. High-Speed Separations on a Microchip. Anal. Chem. **1994**, *66* (7), 1114–1118.
5. Terry, S.C.; Jerman, J.H.; Angell, J.B. A Gas Chromatographic Air Analyzer Fabricated on a Silicon-Wafer. IEEE Trans. Elec. Dev. **1979**, *26* (12), 1880–1886.
6. Burns, M.A.; Johnson, B.N.; Brahmasandra, S.N.; Handique, K.; Webster, J.R.; Krishnan, M.; Sammarco, T.S.; Man, P.M.; Jones, D.; Heldsinger, D.; Mastrangelo, C.H.; Burke, D.T. An Integrated Nanoliter DNA Analysis Device. Science **1998**, *282*, 484–487.
7. Chiem, N.; Harrison, D.J. Microchip-Based Capillary Electrophoresis for Immunoassays: Analysis of Monoclonal Antibodies and Theophylline. Anal. Chem. **1997**, *69* (3), 373–378.
8. Jacobson, S.C.; Hergenroder, R.; Koutny, L.B.; Warckman, R.J.; Ramsey, J.M. Effects of Injection Schemes and Column Geometry on the Performance of Microchip Electrophoresis Devices. Anal. Chem. **1994**, *66* (7), 1107–1113.
9. Jacobson, S.C.; Ramsey, J.M. Microfabricated Devices for Performing Capillary Electrophoresis. In *Handbook of Capillary Electrophoresis*, 2nd Ed.; Landers, J.P., Ed.; CRC Press: Boca Raton, FL, 1997; 827–840.
10. Jacobson, S.C.; Hergenroder, R.; Koutny, L.B.; Ramsey, J.M. Open Channel Electrochromatography on a Microchip. Anal. Chem. **1994**, *66* (14), 2369–2373.
11. Kutter, J.P.; Jacobson, S.C.; Ramsey, J.M. Integrated Microchip Device with Electrokinetically Controlled Solvent Mixing for Isocratic and

Gradient Elution in Micellar Electrokinetic Chromatography. Anal. Chem. **1997**, *69* (24), 5165–5171.
12. Moore, A.W.; Jacobson, S.C.; Ramsey, J.M. Microchip Separations of Neutral Species via Micellar Electrokinetic Capillary Chromatography. Anal. Chem. **1995**, *67* (22), 4184–4189.
13. von Heeren, F.; Verpoorte, E.; Manz, A.; Thormann, W. Micellar Electrokinetic Chromatography Separation and Analyses of Biological Samples on a Cyclic Planar Microstructure. Anal. Chem. **1996**, *68* (13), 2044–2053.
14. Guiochon, G. Conventional Packed Columns vs. Packed Open Tubular Microcolumns in Liquid Chromatography. Anal. Chem. **1981**, *53* (9), 1318–1325.
15. Giddings, J.C.; Chang, J.P.; Myers, M.N.; Davis, J.M.; Caldwell, K.D. Capillary Liquid Chromatography in Field Flow Fraction-Type Channels. J. Chromatogr. **1983**, *255*, 359–379.
16. Kang, Q.; Golubovic, N.C.; Pinto, N.G.; Henderson, H.T. A Novel Integrated Micro Ion-Exchange Separator and Detector on a Silicon Wafer. Chem. Eng. Sci. **2001**, *56* (11), 3409–3420.
17. Henderson, H.T.; deGouvea-Pinto, N. Liquid Chromatograph on a Chip. US Patent 6,258,263B1, July 10, 2001.
18. Golay, M.J.E. Theory of Chromatography in Open and Coated Tubular Columns with Round and Rectangular Cross-Sections. In *Gas Chromatography*; Desty, D.H., Ed.; Academic Press: New York, 1958; 36–54.
19. Halasz, I. Mass Transfer in Ideal and Geometrically Deformed Open Tubes. J. Chromatogr. **1979**, *173*, 229–247.
20. Jorgenson, J.W.; Guthrie, E.J. Liquid Chromatography in Open Tubular Columns: Theory of Column Optimization with Limited Pressure and Analysis Time, and Fabrication of Chemically Bonded Reversed-Phase Columns on Etched Borosilicate Glass Capillaries. J. Chromatogr. **1983**, *255*, 335–348.
21. Knox, J.H. Theoretical Aspects of LC with Packed and Open Small Bore Columns. J. Chromatogr. Sci. **1980**, *18*, 453–461.
22. Knox, J.H.; Gilbert, M.T. Kinetic Optimization of Straight Open-Tubular Liquid Chromatography. J. Chromatogr. **1979**, *186*, 405–418.
23. Vahey, P.G.; Park, S.H.; Marquardt, B.J.; Xia, Y.; Burgess, L.W.; Synovec, R.E. Development of a Positive Pressure Driven Micro-fabricated Liquid Chromatographic Analyzer Through Rapid-Prototyping with Poly(Di-Methylsiloxane) Optimizing Chromatographic Efficiency with Sub-nanoliter Injection. Talanta **2000**, *51*, 1205–1212.
24. Zhang, X.; Regnier, F.E. Analysis of Channel-Geometry Effects on Separation Efficiency in Rectangular-Capillary Electrochromatography Columns. J. Chromatogr. A **2000**, *869*, 319–328.

25. Spangler, G.E. Height Equivalent to a Theoretical Plate Theory for Rectangular GC Columns. Anal. Chem. **1998**, *70* (22), 4805–4816.
26. Thomas, J.W. *Numerical Partial Differential Equations: Finite Difference Methods*; Springer: New York, 1995.
27. Robinson, R.A.; Stokes, D.H. *Electrolyte Solutions*, 2nd Ed.; Butterworths: London, 1970.
28. Kang, Q. A Miniaturized Ion-Exchange Chromatograph on a Silicon Wafer. M.S. Thesis, University of Cincinnati, Cincinnati, OH.
29. Hamilton, R.J.; Sewell, P.A. *Introduction to High Performance Liquid Chromatography*, 2nd Ed.; Chapman and Hall: New York, 1982.

Received September 2001
Revised February 2002